ufop

UFOP PUBLICATION | BIODIESEL & CO.

FINAL REPORT

Biodiesel as an integral component of pioneering diesel fuels

Authors
Martin Unglert, Susanne Proschke, Georg Kröner, Olaf Schröder, Markus Jakob
Coburg University of Applied Sciences

HOCHSCHULE COBURG

Research Project Final Report

Biodiesel as an integral component of pioneering diesel fuels

Edited by: Martin Unglert
                    Susanne Proschke
                    Georg Kröner
                    Olaf Schröder
                    Markus Jakob

Contents

1 Introduction

Use of regeneratively produced fuels is a core aspect of sustainable mobility development [1,2,3,4,5]. Regeneratively produced fuels provide potential independence from fossil energy sources and alternative fuel properties that can be used to optimise engine combustion[6,7]. However, in order to be able to cover the energy requirements of individual mobility, various alternative state of the art fuels will have to be used concurrently on the market. This concurrent use of different fuel types creates the technical dilemma that unfavourable fuel combinations can lead to unwanted segregation and ageing processes in the tank. These processes must be examined and understood in detail.

The research project presented here, "Biodiesel as an integral component of pioneering diesel fuels", examines the segregation and ageing processes of three promising, alternative diesel engine fuels. These fuels are hydrogenated vegetable oils (HVO), polyoxymethylene dimethyl ether (OME) and rapeseed methyl ester (RME), which are described in Chapter 2.1[8,9]. In these fuels, segregation can occur very easily depending on their composition. Therefore, RME is examined in the context of these studies as a solubiliser between HVO and OME.

The studies in this report are divided into two parts. The first part studies blends of the three aforementioned fuels in terms of their segregation stability. Both experimental and numerical approaches will be used to do this. The second part studies the ageing phenomena of selected fuel blends. In both studies, particular attention is paid to the use of increased RME admixtures and their effect on blend and ageing stability.

2   Material and methods

The studies of this project include both experimental and numerical approaches. In order to be able to interpret the results of the studies conducted in Chapters 3 and 4, Chapter 2 first describes the fuels and measurement methods used.

2.1   Fuels used

During the course of this project, the blending and ageing processes of various alternative diesel engine fuels are studied. Table 1 presents an overview of the fuels studied, indicating not only the fuel type and additivation, but additional descriptions and sources of supply as well in order to be able to ensure an unambiguous correlation. The miscibility studies in Chapter 3.2. and the ageing studies in Chapter 4 involve tests and calculations made solely with unadditivated fuels. In order to be able to exclude cross-influences of the additive components, the unadditive fuels are used to study the ageing processes. With regard to OME fuel, it is emphasised that the composition may vary considerably from batch to batch, both in terms of additivation and the production of the base fuel. The results presented in this project refer to the fuels defined in more detail below.

Table 1: Overview of the fuels used.

Fuel	Additivation	Description	Reference
Rapeseed methyl ester (RME)	unadditivated	Not distilled; contains natural antioxidants	ASG
Hydrogenated vegetable oil (HVO)	unadditivated	Isomerised via the Neste procedure	Neste
Polyoxymethylene dimethyl ether (OME)	unadditivated	Contains OME_3 to OME_6	ASG
Stearic acid methyl ester (C18:0)	unadditivated	Laboratory chemical	Sigma-Aldrich

The unadditivated HVO contains the middle-distillate fraction of iso- and n-paraffinic hydrocarbons. The maximum total aromatic content is one percent per weight. The boiling range is between 180 and 320 °C (EN ISO 3405), the flash point is >61 °C, and the ignition temperature is 204 °C. The unadditivated RME meets the requirements of DIN EN 14214. The composition of the unadditivated OME according to the safety data sheet is 40-80 % OME_3, 15-40% OME_4, 0-20 % OME_5 and 0-9.9 % OME_6. The initial boiling point (EN ISO 3405) is 150 °C, and the flash point (DIN EN ISO 2719) is >50 °C. Stearic acid methyl ester is used with a purity of ≥96 %. The melting range is between 37 and 41 °C, and the boiling point is 181-182 °C. Refer to the literature for additional properties and information.[1,3,4,7]

2.2 Measurement methods used

The experimental studies in this project are based on dielectric relaxation spectroscopy and infrared spectroscopy. Both measuring principles are explained below before the measurement results are interpreted in Chapters 3 and 4.

2.2.1 Permittivity

Permittivity describes the electrodynamic permeability of a medium for electric (alternating) fields, whereby the permeability is influenced by the properties of the medium. Permittivity sensors are generally based on electrical capacitors in which two electrically conductive surfaces are exposed to an alternating current. If a dielectric is inserted between the capacitor plates, the dielectric parameters change according to the incurred polarisation effects. Four different polarisation types are distinguished here (electron, interface, orientation and ion polarisation). Electron polarisation is based on an interaction between electric fields and the electron shell. Polar compounds possess a permanent dipole moment that causes the dipoles to be oriented in the alternating field according to the applied field. Nonpolar compounds do not exhibit any orientation polarisation, whereby nonpolar compounds exhibit small permittivity values, and polar compounds larger values. This allows polar and nonpolar compounds to be differentiated based on the magnitude of the relative permittivity. Ion polarisation refers to the displacement of negatively and positively charged particles in the electric field. To minimise the influence of interface polarisation on the measurement, the measurement was evaluated at 1 MHz.

Relative permittivity is defined by the quotient of the capacitance of the medium $C(\omega, T)$ and the empty capacitance $C_0(\omega, T)$, whereby ω is the frequency of the alternating voltage and T is the temperature (equation 1).

$$\varepsilon_r{}'(\omega, T) = \frac{C(\omega, T)}{C_0(\omega, T)} \qquad (1)$$

Moreover, permittivity is a complex-valued function comprising the real part $\varepsilon_r{}'(\omega, T)$ and its imaginary part $\varepsilon_r{}''(\omega, T)$ (equation 2). The real part (relative permittivity) is influenced by the polarisation effects, whereas the imaginary part $\varepsilon_r{}''(\omega, T)$ reflects the resulting losses in polarisation and conductivity.

$$\varepsilon_r(\omega, T) = \varepsilon_r{}'(\omega, T) - j\varepsilon_r{}''(\omega, T) \qquad (2)$$

For permittivity measurements, a cylindrical capacitor is used, in which field lines outside the sample volume are derived by a so-called protective ring arrangement. The measured capacitance thus lies solely in the sample, whereby equation 1 can be used to determine permittivity. Measurements were made with an impedance analyser (Keysight E4990A), which determines the capacitance and dissipation factor. The frequency of the alternating voltage is modulated in a range between 200 Hz and 120 MHz, whereby the values of the relative permittivity are stated at 1 MHz as standard. Using a temperature controller (Belektronig HAT control; temperature sensor PT100) and external cooling, all measurements were conducted at 25 °C.

2.2.2 Infrared spectroscopy

In infrared spectroscopy, electromagnetic radiation of defined wavelengths is passed through a sample to be studied. Within the sample, molecules absorb the radiation at molecule-specific wavelengths, so that the analysis of the emitted radiation allows conclusions to be drawn about the molecule groups. This analysis method thus not only allows individual molecule groups to be identified, but allows changes in the molecule groups caused by ageing processes, for example, to be studied as well.

Changes in the functional groups during the ageing and resulting from the auto-oxidation of fuels are measured with a Fourier Transform Infrared Spectrometer (FTIR), Nicolet 6700 FTIR from Thermo Scientific according to the ATR measurement principle. The spectra are recorded in the 4000 cm^{-1} and 650 cm^{-1} range with 16-fold multiple determination. The measured data is evaluated using the Omnic software from Thermo Scientific.

2.3 Ageing methods used

An ageing apparatus developed at Coburg University of Applied Sciences is used in the course of these studies that enables the simultaneous ageing of large and sometimes highly volatile fuels. This ageing apparatus is illustrated in Fig. 1 and is composed of three parts. The first part of the apparatus (Fig.1 left) is equipped with an air supply with a defined volume flow control. This control is set to a constant 10 L/h air supply in order to be able to exclude cross influences due to varying air volume flows. Part 2 of the ageing apparatus (Fig. 1, centre) features an air dehumidification system consisting of a water separator, a molecular sieve and a potassium hydroxide filter. This air dehumidification is necessary in order to be able to adjust the input and thus

6

the influence of the incoming humidity in a defined way. This configuration allows the relative humidity (RH) of the air flowing through it at an inlet temperature of 25 °C to be reduced from 50 to 15 %.
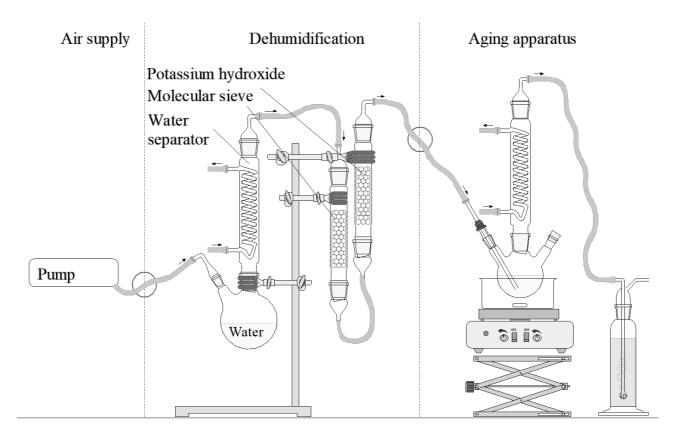

Fig. 1: Sketch of the ageing apparatus with air dehumidification.

The third part of the ageing setup, shown on the right in Fig. 1, contains the actual ageing apparatus, which is based on the Rancimat ageing procedure. In this setup, fuel samples are heated and simultaneously mixed with the dehumidified air volume flow. At this point, the fuel sample is exposed to elevated temperatures of 110 °C and to 10 L/h air flow for a defined period of 120 hours in order to age the sample artificially. To prevent volatile components from evaporating from the system, the ageing apparatus outlet is equipped with a reflux condenser. In case volatile fuel components evaporate, they are condensed at the reflux cooler and drop back into the sample again. The described apparatus thus permits controlled sample ageing under defined boundary conditions of duration, temperature, humidity, even of highly volatile compounds, and is thus the basis of the experiments in Chapter 4. The depicted ageing apparatus must be used because only significantly smaller sample volumes and no highly volatile

compounds can be aged with the standard methods such as the Rancimat method, for example. Samples are aged with 220 mL in the depicted setup as part of the studies presented here.

3 Test results

As already described in the introduction, this project consists of studies into the blend and ageing stabilities of OME, HVO and RME (or OME, HVO and C18:0) blends. The following two subchapters first describe the underlying principles of the studies into blend and ageing stability before the potential of the RME (or C18:0) admixture as a solubiliser is subsequently discussed.

3.1 Segregation studies

3.1.1 The Hansen solubility parameter theory

The Hansen solubility parameter theory states that different liquids only mix without phase separation if the pure substances do not differ significantly from each other in terms of their specific properties. The properties considered relevant in Hansen's theory are the hydrogen bond, polarity and London interactions of the individual substances, which are described in detail below.

- Hydrogen bonds:
  Attractive interaction between a covalently bonded hydrogen atom and a free electron pair. The hydrogen atom must be polar bonded.

- Dipole-dipole interaction:
  Forces between molecules with a permanent electric dipole moment. The intensity of the interaction exceeds the London interactions.

- London interaction:
  Weak forces of attraction between nonpolar and polar molecules caused by the formation of spontaneous and induced dipoles.

The Hansen solubility parameter theory is based on an analysis of the cohesive energy density (δ) (equation 3). Using the ideal gas constant (R), molar volume (V_m),

temperature (T) and evaporation enthalpy (ΔH_v), the cohesive energy density describes the energy required to cause a given volume of molecules to separate infinitely from its neighbouring molecules.[10][11]

$$\delta = \sqrt{\frac{\Delta Hv - RT}{Vm}} \tag{3}$$

The Hansen solubility parameters divide, according to the three described intermolecular interactions, the cohesive energy density into the proportions of the three parameters: London interactions (δD), polar interactions (δP), and hydrogen bonds (δH) (equation 4).

$$\delta = \delta D + \delta P + \delta H \tag{4}$$

The extent to which two liquids to be mixed can differ without segregation, or when a solid dissolves completely in the solvent, is described by the relative segregation radius according to formula (5) and (6).

$$R_a{}^2 = 4 * (\delta D1 - \delta D2)^2 + (\delta P1 - \delta P2)^2 + (\delta H1 - \delta H2)^2 \tag{5}$$

$$RED = R_a / R_0 \tag{6}$$

The London interaction forces δD, dipole interactions δP, and hydrogen bonds δH of liquid 1 and 2 are entered in formula (5). It is evident that the corresponding parameters of the two liquids are subtracted, the individual differences squared, and the squares of the individual differences summed up. Geometrically, this means that the distance between points in space is determined in a 3-dimensional coordinate system, and thus Ra can be interpreted as the radius of a sphere. This radius describes the sum of all parameter differences, and thus represents the forces that can lead to segregation. The factor 4 of the London interaction forces in formula (5) is determined empirically and

describes the disproportionately high proportion of these forces in segregation processes.

At the end of the calculations, the Ra value is compared with an empirically determined R_0 parameter (equation 6), which describes by when a blend can be present. The resulting ratio of R_a and R_0 is called the relative energy distance (RED), where the limit between blending and segregation is defined at RED = 1.[10][11]

RED < 1:   complete blend
RED = 1:   partial blend
RED > 1:   no blend

3.1.2 Experimental segregation studies

The Hansen solubility parameters at 25 °C are already available in the literature for many solvents[12]. The Hansen solubility parameters and R_0 values have not yet been studied for regeneratively produced fuels such as RME, OME or HVO. Therefore, the experimental part of these studies evaluates the blends of solvents and fuels at 25 °C as a comparison using the dual control principle to determine whether there is phase separation or miscibility.

To illustrate segregation, Fig. 2 shows a series of blends of HVO and OME in which the HVO admixture increases from left to right in steps of 10 vol% respectively. The sample on the far left therefore contains 90 vol% OME and 10 vol% HVO, while the blending ratio is reversed in the sample on the far right. It can be seen that blends with 20 to 70 vol% OME content (2-7 sample from left) form two liquid phases. Since this phase separation, according to Hansen's theory, is based on highly different fuel properties, two miscible liquids must be comparable in terms of the Hansen solubility parameters. Using this logic as a basis, the Hansen solubility parameters of the liquids not yet tabulated can be derived by blend tests with known liquids.
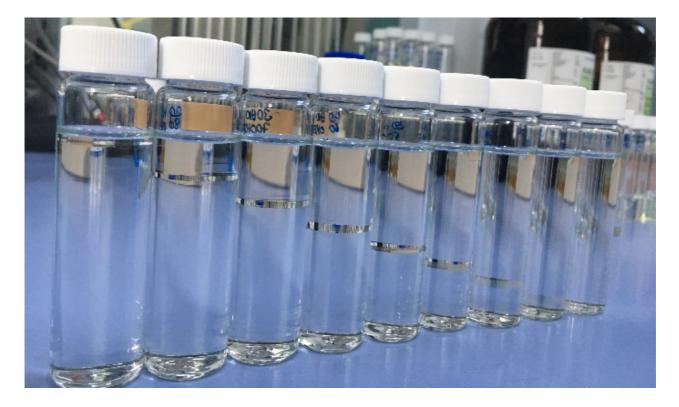
Fig. 2: HVO/OME series of blends with phase separation at room temperature (increase of HVO content from 10% to 90% in 10% increments from left to right).

Table 2 lists the Hansen solubility parameters and interaction radii of the studied fuels. Here it is evident that the resulting polarity parameters δP of the HVO fuels differ greatly from the value of the OME fuel. This result likewise represents the segregations in Fig. 2 with reference to Hansen's theory in Chapter 3.1. Moreover, it is evident that the Hansen solubility parameters of RME fuels each lie between the parameters of OME and HVO. Therefore, it is possible that phase separations as shown in Fig. 2 with three-component blends of RME, OME and HVO could be avoided. This effect will be studied further in the following report.

Table 2: Hansen solubility parameters of selected fuels.

Sample	Temperature	δD	δP	δH	R_0
HVO unadd	25 °C	16.8	0	0	11.5
RME unadd	25°C	15	7.5	7	6.2
OME unadd	25 °C	16.2	9.3	7	12.2
C18:0	25 °C	15.5	6	7	9.5
HVO add	25 °C	17	0	0	12.9
RME add	25 °C	17	5.3	2.6	6.2
OME add	25 °C	16.5	7.2	4.1	13

One last important detail from Table 2 regards the differences between different batches of fuels. It should be explicitly stated at this point that the Hansen solubility parameters for exactly the batch to be studied are collected for a very precise investigation of the miscibility (e.g. the temperature dependence of the phase separation). This is illustrated by the differences in the Hansen solubility parameters in Table 2 from the additivated fuels to the unadditivated fuels. It should be emphasised that the fuels differ not only as regards additivation, but also as regards the basic substance. Therefore, the differences in Table 2 cannot be solely attributed to the influence of the composition or additivation. It is evident, however, that the Hansen solubility parameters of the additivated and unadditivated batches do not differ by orders of magnitude. This means that general statements on miscibility with good or poor miscibility can to a certain extent be applied to other batches with similar Hansen solubility parameters. No statement is possible only in the limit range of the miscibility. Nevertheless, it must be noted that the Hansen solubility parameters may not be adopted for fuel samples from other production batches without adjustment or control.

3.1.3 Numerical segregation studies

The results from Chapter 3.1.2 are limited to the extent that the experimentally generated results can only be applied for 25 °C. In order to avoid this temperature limitation, the results from Chapter 3.2 are temperature corrected using formulae from the literature[13] (equations 7 to 9). The α factor is referred to as the coefficient of linear expansion and allows the Hansen solubility parameters to be extrapolated to lower or higher temperatures. The given calculation formulas are based on the assumption that the Hansen solubility parameters according to equation 1 correlate with the molar volume, and that the parameter α can be calculated by the quotients of the sample density.[13] Since the sample densities at different temperatures are easily determinable experimentally, this approach allows a simple extrapolation option for existing parameters. The temperature influence depends on the temperature difference, the coefficient of linear expansion α, and on an empirically determined factor that differs for each of the three Hansen solubility parameters.

$$\delta D_T = \delta D * (1 - \Delta T * \alpha_{mittl.} * 1{,}25) \tag{7}$$

$$\delta P_T = \delta P * (1 - \Delta T * \frac{\alpha_{mittl.}}{2}) \tag{8}$$

$$\delta H_T = \delta H * \left(1 - \Delta T * \left(0{,}00122 + \frac{\alpha_{mittl.}}{2}\right)\right) \tag{9}$$

$$\alpha_{mittl.} = \frac{\sqrt[3]{\left(\frac{\rho_0}{\rho_2}\right)} - 1}{\Delta T} \tag{10}$$

Equations 7-9 reveal that all temperature correction functions contain a correction factor of the form $(1 - \Delta T * x)$ with $\Delta T = T - T_0)$. This means that an increase in temperature $(\Delta T > 0)$ leads to reduced, temperature corrected Hansen solubility parameters (Index T). Geometrically, this means that the blending ranges, which can be imagined as spheres in a three-dimensional coordinate system, move closer to the centre. Since the R_0 interaction radii are not temperature corrected, the shift of the centre points means a higher probability of overlap (RED < 1) and thus represents an improved miscibility of liquid media at elevated temperatures.

Table 3: Temperature corrected Hansen solubility parameters of unaged fuels at temperatures from -20 to 40 °C.

Sample	Temperature	δD	δP	δH	R_0
HVO unadd	40 °C	16.5	0	0	11.5
	25 °C	16.8	0	0	11.5
	10 °C	17.1	0	0	11.5
	-5 °C	17.4	0	0	11.5
	-20 °C	17.7	0	0	11.5
RME unadd	40 °C	14.8	7.5	6.8	6.2
	25°C	15	7.5	7	6.2
	10 °C	15.2	7.5	7.2	6.2
	-5 °C	15.4	7.6	7.3	6.2
	-20 °C	15.6	7.6	7.5	6.2
OME unadd	40 °C	15.8	9.2	6.8	12.2
	25 °C	16.2	9.3	7	12.2
	10 °C	16.5	9.4	7.2	12.2
	-5 °C	16.9	9.5	7.3	12.2
	-20 °C	17.2	9.5	7.5	12.2
C18:0	40 °C	15.3	6	6.8	9.5
	25 °C	15.5	6	7	9.5
	10 °C	15.7	6	7.2	9.5
	-5 °C	15.9	6	7.3	9.5
	-20 °C	16	6.1	7.5	9.5

Table 3 lists the temperature corrected Hansen solubility parameters of the fuels studied for 5 exemplary temperatures between -20 and 40 °C. It should be emphasised that the R_0 interaction radii are the same at all temperatures, since there is no temperature correction function for the interaction radius.

It is evident that the three Hansen solubility parameters, according to equation 7-9, are influenced differently by the temperature. The changes are in the -20 to 40 °C range of maximum 10 % at δD. The parameter changes of δP and δH are lower. Particularly noteworthy here are fuels such as HVO, for which the experimentally derived Hansen solubility parameters δP and δH are already zero at 25 °C and thus the temperature-corrected values are zero as well (multiplying by 0).

Based on the generated Hansen solubility parameters, the desegregation stabilities of different ternary blends of HVO, OME and RME (or HVO, OME and C18:0) can be calculated for different temperatures. It should be noted that the evaluations first calculate the blends of HVO and OME and then the admixture of RME, as the results of this calculation method provide the most consistent experimental results.
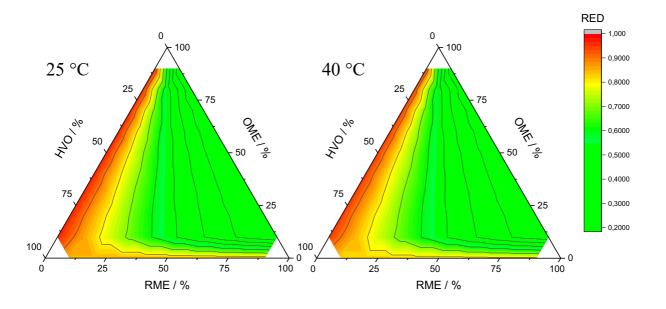

Fig. 3: Relative energy distance (RED) for blends of unaged RME, OME and HVO at 40 °C (left) and 25 °C (right).

Fig. 3 shows the results of the Hansen calculations of OME, HVO and RME blends at 25 °C (left) and 40 °C (right) in so-called simplex diagrams. In these simplex diagrams, each side of the triangle corresponds to an axis that represents the respective admixture of the components from 0 to 100 vol%. The corners of the triangle thus contain the respective pure fuels, which are not taken into account in these simulations and are

therefore not highlighted in colour. One point in the simplex is composed using an imaginary continuation of the positioned axis markings. All the points with the same proportion of the component of the respective axis lie on these imaginary lines. This blend with 33.3 vol% respectively of the three components is depicted in the middle of the triangle, and the blends with low RME proportions on the left edge of the triangle. The colour scale depicted on the right in Fig. 4, scaled from red at RED ~ 1, which corresponds to segregation, to green at RED < 0.75, at which no segregation tendency exists.

The calculated results in Fig. 3 show on the basis of the areas depicted in red on the left edge of the diagrams that there is a high risk of phase separation with no or low RME admixtures. This result is in accord with experimental observations such as those in Fig. 2 and is thus a first indication of the robustness of Hansen's calculations. Moreover, Fig. 3 reveals that increased RME admixtures lead to a reduction of the RED value and thus to an improvement of the blend stability. This means that the thesis posited at the beginning, stating that RME can improve the blend stability of HVO, OME and RME blends as a solubiliser, is numerically/theoretically proven. These effects as well are validated and confirmed in a further experiment, which will not be discussed in detail here because of their scope. The results of the numerical and experimental studies prove, however, that RME has a positive influence on the blending stability of RME, HVO and OME blends. The described Hansen parameter theory now provides a theoretical basis for describing these effects as well.

Besides the blend stabilities of RME, HVO and OME at 25 °C, depicted on the left in Fig. 3, the evaluations of the temperature corrected Hansen solubility parameters at 40 °C are depicted on the right in Fig. 3 as well. At first glance, it is evident that the general statements do not change significantly as a result of the temperature corrections, which is obvious since the Hansen solubility parameters in Table 3 likewise do not undergo significant changes as a result of the temperature correction. Upon closer inspection, it is evident that the position of individual isolines is slightly changed, so that a closer inspection of the differences is necessary.

In order to more clearly illustrate the effect of the temperature correction, the difference map of the two simplex diagrams is depicted in Fig. 4. The axis labels and scales from Fig. 4 are identical to Fig. 3. In order to clearly distinguish the absolute and difference maps, a different colour scale is selected in Fig. 4, which scales the difference values from 0.012 (darker) to 0.006 (lighter). Values smaller than 0 are not possible when scaling to 40 °C, as the correction formulas respectively contain the factor $(1 - \Delta T * x)$)

and thus the values at 40 °C are always smaller (or the same when the Hansen solubility parameter value is zero) than the values at 25 °C.
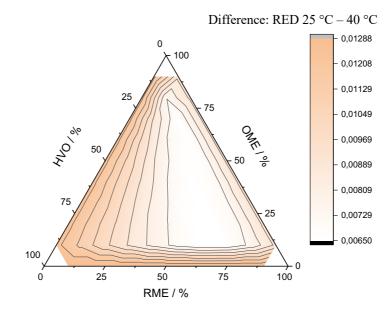

Fig. 4: Differences drawing between 25 and 40 °C of the blends of unaged RME, OME and HVO.

A bright area is depicted in the middle of Fig. 4, where a slight improvement in miscibility is evident from scaling the temperature from 25 to 40 °C. However, it is important that this area in Fig. 3 is already within the area marked in green, where stable blends of the unaged samples can already be achieved by admixing RME. That is why the slight improvement in miscibility from 25 °C to 40 °C is not a technically relevant advantage. From the bright area in the middle of Fig. 4, however, one can see that greater miscibility advantages from increasing the temperature are depicted towards the axes. It should be emphasised once more that the areas along the axes represent blends with two components, where the left axis depicts the critical blend of HVO and OME. This means that the advantages of increasing the temperature to 40 °C for the blends of OME and RME or of HVO and RME do not represent a technical advantage either since segregation-stable samples in the unaged state are already predicted here in Fig. 3 as well. In contrast, the segregation critical samples of HVO and OME are depicted along the left axis. In this range, RED is close to one. It becomes clear here that the small changes between 25 and 40 °C determine whether the RED is above or below RED = 1. The differences drawing makes it evident that an improvement in miscibility is predicted by increasing the temperature (RED(25°C) -

RED(40°C) > 0). This means that the temperature scaled Hansen model predicts improved miscibilities, which are validated by random measurements in this project.

As described in the introduction already, not only are blends of OME, HVO and RME taken into account in these simulations, but blends of OME, HVO and C18:0 as well. The main difference between C18:0 and RME is the proportion of unsaturated fatty acid methyl esters, which are not contained in C18:0. Consequently, a comparison of the results of C18:0 and RME reveals the influence of saturated and unsaturated fatty acids within the ternary blends. This influence of fatty acid methyl esters is studied further in Chapter 4 with regard to ageing stability.

Fig. 5: Relative energy distance (RED) for blends of unaged C18:0, OME and HVO at 25 °C (left) and 40 °C (right).

Fig. 5 depicts the simplex diagrams of the calculated RED miscibility values of unaged HVO, OME and C18:0 fuels for 25 °C (left) and 40 °C (right). When compared to Fig. 3, it is evident that the C18:0 admixture (Fig. 5) does not result in significant changes when compared to RME (Fig. 3). The ranges marked in red along the right axis show in both cases the blend-unstable HVO-OME systems, where the C18:0 or RME content is very low. For ternary blends with more than ~ 25 vol% C18:0 content, stable blends of the unaged components with RED < 1 are depicted in Fig. 5 as well. This result means that both RME and C18:0 can be used as solubilisers for unaged ternary blends with OME and HVO. This correlation is plausible since RME and C18:0 differ only in the proportion of unsaturated fatty acid methyl esters, which has no significant influence on the polarity of the fuels in unaged samples.

To illustrate the differences between C18:0 and RME, Fig. 6 depicts the difference maps of the C18:0 simplex diagrams of 40 and 25 °C. Fig. 6 is thus complementary to Fig. 4, which depicts the corresponding simplex diagrams of the RME systems. When comparing Fig. 4 and 6, it is evident that only RED difference values > 0 are calculated in Fig. 6 as well, as already described by the calculation formulas in Chapter 3.3. Furthermore, it is evident that a more homogeneous curve progression of the RED differences is depicted in Fig. 6 than in Fig. 4. For ternary blends with C18:0, the maximum difference in the RED between 25 and 40 °C is approx. 2 %. The temperature influence on the RED decreases from left to right in the simplex with the increasing content of C18:0. The exception is the binary blends of HVO and C18:0. Here, the temperature influence on the RED increases between 0 and 10 % OME towards the binary HVO/C18:0 blend. The binary blends of OME and C18:0 exhibit the least temperature influence on the RED.
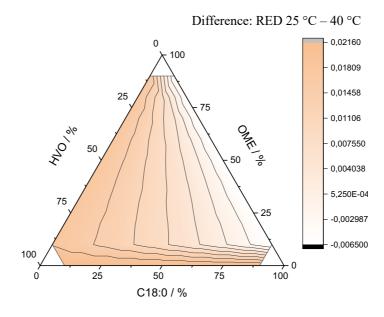

Fig. 6: Differences drawing of the ternary blends with C18:0. Depicted are the differences of the RED between 25 and 40 °C.

To conclude, Fig.7 shows the differences between the RED maps of HVO, OME, RME blends and HVO, OME, C18:0 blends at 25°C respectively. In this case, it is evident at the lower edge of the differential map that the blend stability of binary blends of unaged HVO and C18:0 or RME is improved by approx. 9 % when using C18:0. However, it must be emphasized here that even the binary blend of the unaged HVO and RME

samples is blend-stable (see Fig. 4) and thus no further technical benefit is generated by the improvement in stability.

A possible explanation is offered by the Hansen solubility parameters, whereby the differences between the three Hansen solubility parameters in C18:0 to HVO compared to RME are fewer. This can be explained by the structure of the molecules. Due to the unsaturated fatty acid methyl esters, RME possesses an angled structure, whereas C18:0 without double bonds has a stretched (non-angled) shape that is more similar to HVO. Following the principle "like dissolves in like", solubility is greater when the geometry is more similar and the resulting stronger attractive interactions of the molecules with each other greater. Greater interaction means better solubility, which is reflected in a small RED.[14] The other range is represented by all other blends in which the RED of RME is lower than that of C18:0. In ternary blends of RME, miscibility of RME is therefore minimally greater than that of C18:0.
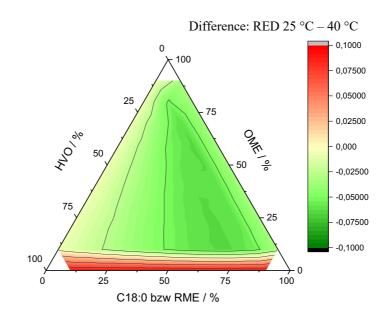

Fig. 7: Differences drawing of the ternary blends between RME and C18:0 at 25 °C.

3.1.4 Crystallisation of C18:0 as limitation for miscibility

To reliably predict miscibility, the blend model must be checked by considering the crystallisation temperature or melting point. Both models predict good miscibility for ternary C18:0 and RME blends. The experiment shows, however, that due to the low melting point of C18:0 at a high C18:0 concentration, crystallisation sets in as early as

at room temperature. The formation of a solid phase precludes its use as a fuel despite good miscibility according to the theory of Hansen solubility parameters. In cases where the fuels exhibit high melting points, the blend model can be used to make a good prediction of miscibility.

3.2 Ageing of ternary fuel blends

As the proportion of plug-in hybrids (PHEV) increases in the future, greater importance will be attached to the ageing stability of fuels. Depending on driving conduct, PHEVs can be driven purely electrically, which means that the fuel in the tank has a significantly longer retention time. An additional complicating factor for future regenerative fuel blends is that the differences in polarity of the individual components and the increasing polarity due to oxidation over the ageing period make it necessary to study miscibility. Therefore, ageing studies of the ternary blends of unadditivated RME, HVO and OME will be carried out in the second part of this project. Additivation is deliberately not included at this point in order to exclude cross-influences of different additive packages and selective effects on only one blend component.

The ageing apparatus described in Chapter 2.2.3. is used to produce the aged samples. Table 4 depicts the parameter of fuel ageing, whereby the fuel blends are aged for 120 h at 110 °C and a 10 L/h air supply. The variation parameters in these ageing studies are air drying quality between 15 and 50 % RH, replacement of RME by C18:0 as a comparison with the data from Chapter 3.1, and the nine compositions of the fuel blends according to Fig.8. This results in a total of 36 aged fuel blends from nine compositions, 2 air drying grades and 2 studied FAME derivatives within the scope of these studies.

Table 4: Parameters of fuel ageing.

Air curing	applied FAME	Ageing duration	Ageing temperature	Air volume
With (15 % RH)	RME			
or	*or*	120 h	110 °C	10 L/h
Without (50 % RH)	C18:0			

Figure 8 depicts the nine studied fuel compositions in a simplex diagram and as a table. Three samples contain 7 vol% RME or C18:0 and reflect fuel blends currently relevant to the market. Since the studies from project part 1 reveal an improved blend stability with increased RME admixture, increased RME admixtures of up to 50 vol% are taken

into account in project part 2 as well. These studies should reveal whether the positive effects of the improved blend stability are offset by negative ageing effects caused by an increase in the RME admixture.
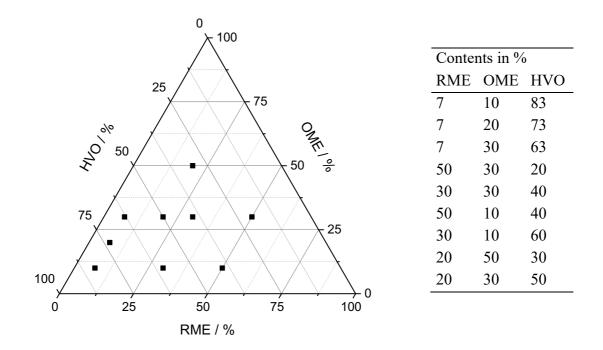

Contents in %		
RME	OME	HVO
7	10	83
7	20	73
7	30	63
50	30	20
30	30	40
50	10	40
30	10	60
20	50	30
20	30	50

Fig. 8: Composition of the aged fuel blends.

3.2.1 Qualitative test of the aged fuel blends

Ageing characterisation of the fuel blends is classified into four successive steps. In step 1, the samples are visually inspected for any noticeable changes, phase separation or discolouration. After this qualitative test, the volume fractions are determined and compared with each other in the second step. In step 3, the FTIR measurements of the individual phases are compared to detect the compositions. In part 4 of the ageing analysis, dielectric relaxation spectroscopy is performed, which is based on the principle of permittivity measurements of the respective samples and which can detect oxidation during the ageing.

The aged samples are visually inspected and assessed in the qualitative ageing characterisation area. Ageing of the fuel blends results in significant differences depending on the sample composition and relative humidity. Ageings differ in colour, phase separation, volume of the upper and lower phases and occurring crystallisation. To this end, Fig. 6 compares three exemplary samples after ageing. The samples shown are aged at 15 % relative humidity, 30 vol% OME and, from left to right, with

increasing RME contents from 7 to 50 vol%. The sample on the left side of Fig. 6 corresponds to 7 vol% RME, which is a fuel blend currently relevant to the market. The picture on the right side of Fig. 6 shows an aged sample with 50 vol% RME. Different effects can be seen on the aged samples in Fig. 6. At 7 vol% RME content (Fig. 6 left), it is evident that ageing causes a phase separation in which the lower phase, in which RME concentrates, turns a brownish colour. The sample with 30 vol% RME (Fig. 6 middle) reveals that the brown discoloured lower phase is significantly larger and thus scales with the RME admixture. When mixed with 50 vol%, no phase separation is evident any more, but the complete blend has a brownish discolouration. At this point it can therefore be assumed that the ageing products which cause the brownish discolouration increase with the RME admixture. The sample shown with 50 vol% RME, 30 vol% OME and 20 vol% HVO (15% RH) is the only one of the 36 ageing samples in this project where no phase separation occurred. The Annex contains pictures of all 36 ageing samples.

Fig. 9: Samples aged at 110 °C for 120 h at 15 % humidity with RME.

Two conclusions can be drawn on the basis of the data. On the one hand, the sample discolourations of the aged samples scale with the proportion of the RME admixture. On the other hand, phase separation occurred in 17 of the 18 RME samples after the ageing. Since phase separation is described by the Hansen solubility parameter theory, it can be concluded from the resulting phase separation that molecular processes may have led to changes in the Hansen solubility parameters due to ageing.
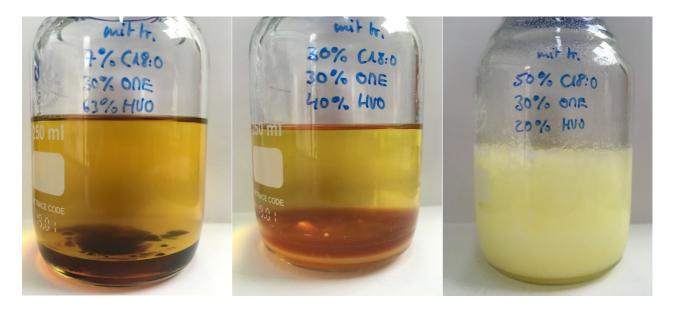
Fig. 10: Samples aged at 110 °C for 120 h at 15 % humidity with C18:0.

Fig. 10 depicts, similar to Fig. 9, the same compositions, except that RME is replaced by C18:0. Differences between RME and C18:0 can be seen in the colouration of the sample with 7 vol% C18:0, 30 vol% OME and 63 vol% HVO. The C18:0 in Fig. 10 exhibits a significantly more pronounced discolouration than the corresponding RME sample in Fig. 9. Moreover, the admixture of C18:0 likewise changes the volume fractions of the phases. The lower phase of the sample with 30 vol% C18:0, 30 vol% OME and 40 vol% HVO has a significantly lower volume content. Particularly noteworthy is the crystallisation that occurs at a 50 % C18:0 content.

It should be repeated here that the blends of the unaged RME or C18:0 samples or the blend stability in the unaged state exhibit small differences, and thus the influence of the unsaturated fatty acid methyl esters in the unaged state is not significant. When comparing the aged samples with RME and C18:0 in Fig. 9 and Fig. 10, a distinct difference is already evident in the qualitative assessments. This means that the influence of the unsaturated fatty acid methyl esters in the ternary sample blends changes significantly due to the ageings, which is studied further in below.
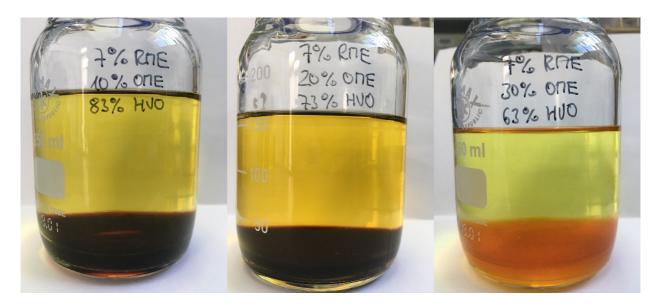
Fig. 11: Samples aged at 110 °C for 120 h at 15 % humidity with RME with a different OME admixture.

Figure 11 depicts three samples with constant RME content and increasing OME content. The OME content increases from left to right in 10 vol% steps. No significant differences are evident between 10 vol% and 20 vol% OME. Distinct differences are evident at a proportion of 30 vol%. Due to the 30 vol% OME content, the lower phase is not black but light brown. The composition of the fuels thus has a considerable influence on the ageing result, in particular on phase separation, the volume fractions of the phases, and on the formation of ageing products, which will be studied in more detail with FTIR and permittivity below.

3.2.2 Volume analysis of the separated phases

The volume fractions of the upper and lower phase of the aged samples (Figure 13) are recorded in the second step of the ageing analysis. The y-axis thereby depicts the volume fraction in percent of the upper and lower phase of a respective aged sample, whose respective initial composition is plotted on the x-axis. The 36 ageing samples can be classified into four groups, whereby the composition of the respective samples is kept constant. The groups differ, on the one hand, in the RME or C18:0 component and, on the other hand, in the relative humidity of the air introduced during the ageing. The designation of the samples is described in the illustrations and in the following text by their composition, using the form: methyl ester content/OME content/HVO content.
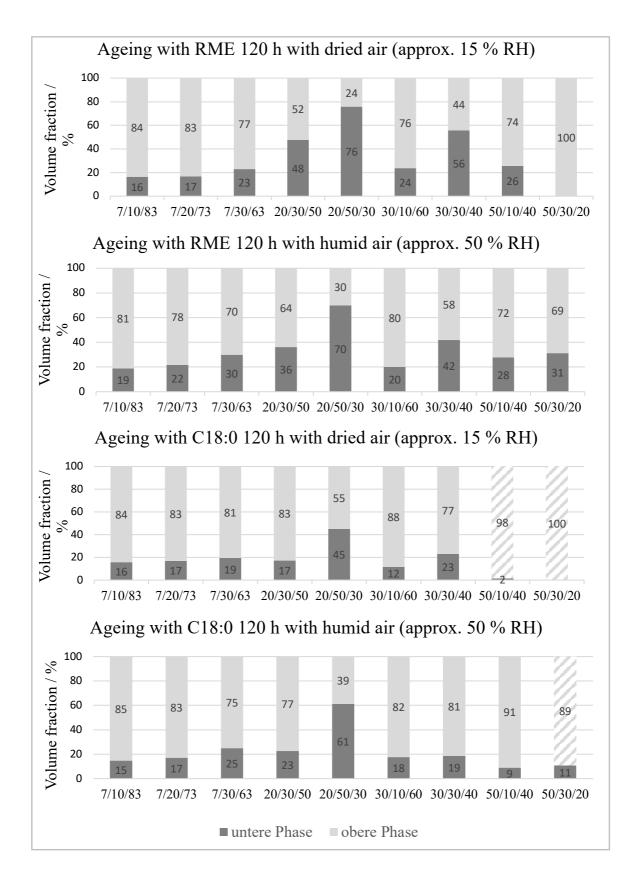
Fig. 12: Volume fractions of the respective phases of the RME or C18:0/OME/HVO samples after ageing 120 h. The cross-hatched samples are present as a solid.

Two samples stand out in the upper group with C18:0 and 50 % RH. When compared to the other samples in this group, phase separation is significantly stronger in 20/50/30

in favour of the lower phase. Of these, 20/50/30 is the only sample with an OME content of 50 %. The other distinctive sample is 50/30/20, whose upper phase is completely solid. The reduction in humidity in group 2 (C18:0, 15 % RH) leads to an additional sample (50/10/40) with a solid upper phase. Due to the lower humidity, the volume fraction of the lower phase is lower in 50/10/40.

When compared to the RME ageings, group 3 and 4, a generally slightly higher proportion of the lower phase is exhibited when compared to C18:0. Sample 20/50/30 also exhibits a high volume fraction of the lower phase for RME, although this is even higher when compared to C18:0. RME has no samples with a solid form. Two samples, 20/30/50 and 30/30/40, differ significantly in the volume fraction of the lower phase when these are compared with the same C18:0 samples.

Overall, the volume fractions of the phases indicate a correlation between the amount of polar fractions of OME and RME/C18:0 and the volume fraction of the lower phase. The higher the combined proportion of RME and OME, the greater the volume fraction of the lower phase. Compared to RME and C18:0, this trend is much more pronounced for RME. Differences between C18:0 and RME are revealed in the Hansen solubility parameters of both components. C18:0 ($\delta P = 6$; $\delta H = 7$; $R_0 = 9.5$), when compared to RME ($\delta P = 7.5$; $\delta H = 7$; $R_0 = 6.2$), produces fewer polar interactions than RME. This results in a better solubility with respect to nonpolar HVO, which means that the proportion of the upper phase after the ageing is greater than with RME. In group 4 with RME and at 15 % RH, 50/30/20 is the only sample without phase separation. For more detailed information on the respective phases, FTIR and permittivity are used in the analysis below.

3.2.3 Infrared spectroscopy

Fig. 13 depicts FTIR transmission spectra of the blend with 30 vol % RME, 30 vol % OME and 40 vol % HVO. Depicted are the respective upper and lower phases after ageing for 120 h at 15 % or 50 % relative humidity.

In the lower phase, the OH band (>3100 cm^{-1}), the carbonyl band (1650 cm^{-1} - 2000 cm^{-1}) and the fingerprint region (less than 1500 cm^{-1}) are much more pronounced than in the upper phase. Conversely, the CH oscillations of the CH, CH$_2$ and CH$_3$ groups are much less pronounced in the lower phase. These differences indicate an increased polarity caused by oxidation products (alcohol groups, aldehydes, ketones, acids and water). While the carbonyl band exhibits only slight differences of different humidity, the OH band is much more intense. On the one hand, these differences result from a

strong acidification and, on the other hand, from a greater induction of water at 50 % RH compared to 15 % RH. In order to evaluate the ageing, the strength of the carbonyl band obtained by integrating the area is examined below. Based on the FTIR analyses, the overall trend is that nonpolar components concentrate in the upper phase during phase separation, whereas polar compounds are present in the lower phase.
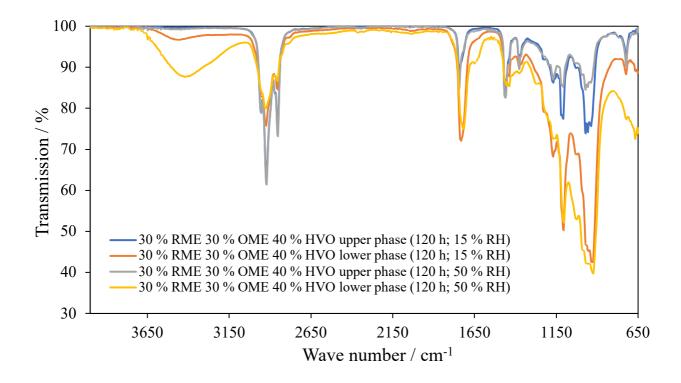

Fig. 13: Infrared spectrum of the different phases after ageing the sample 30 % RME, 30 % OME, and 40 % HVO for 120 h at 15 and 50 % RH.

In order to characterise the ageing condition of the samples, these must be taken into account as well due to the phase separation that occurs. To do this, the FTIR spectra are integrated in the wave number range of the carbonyl band from 1580 to 1880 cm^{-1}. The integrated range of the FTIR measurements is multiplied by the respective volume fraction of the measured phase and the value of the unaged sample is subtracted (equation 9 and 10). In so doing, ageing of the upper and lower phase is determined (Fig. 14).
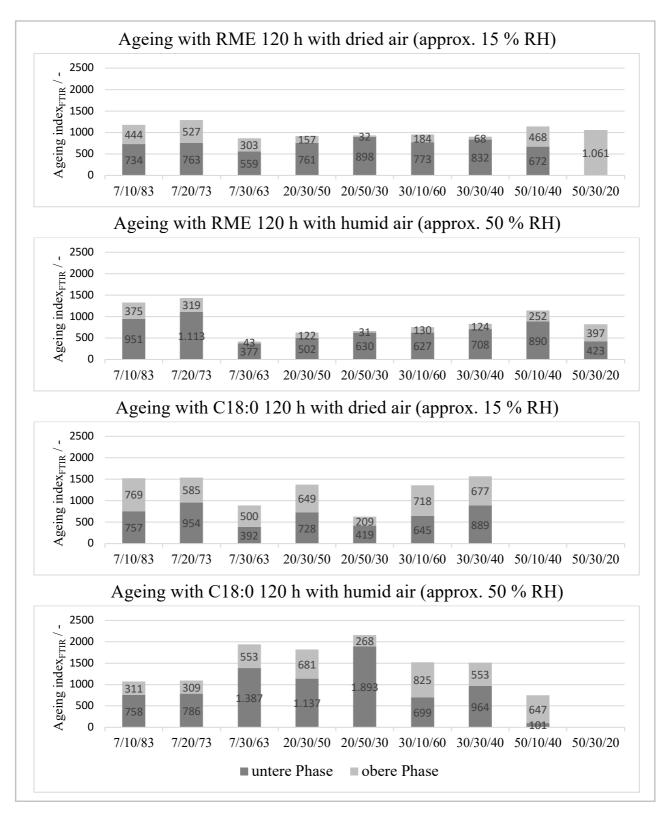
$$\text{Ageing index}_{\text{upper phase}} = (\text{FTIR}_{\text{upper phase}} - \text{FTIR}_{\text{0h}}) \cdot \varphi_{\text{upper phase}} \qquad (9)$$

$$\text{Ageing index}_{\text{lower phase}} = (\text{FTIR}_{\text{lower phase}} - \text{FTIR}_{\text{0h}}) \cdot \varphi_{\text{lower phase}} \qquad (10)$$

27

This evaluation makes it possible to compare the individual samples, even if they have different volume fractions of the upper and lower phase. No comparable data can be collected for the samples that have crystallised out after the ageing. The value of the ageing is to be regarded as a relative parameter here, which allows the samples studied here to be compared with each other. As already depicted in Fig. 13, the ageing is divided into four categories with the volume fractions. This is done in C18:0 and RME or 15 and 50 % RH respectively. The 20/50/30 sample ages by far the least in the C18:0 ageing series at 15 % RH. In the samples with a low RME content (7% and 20%), an increase in the OME content causes the ageing to decrease. With 30 % C18:0, the influence is then the opposite. To interpret the influence of C18:0 and OME on the ageing, the miscibility model in Fig. 6 offers an explanation. This describes considerably poorer miscibility at low admixtures of C18:0 and OME. If the admixtures of OME and C18:0 are increased respectively to approx. 30 %, then miscibility is significantly improved. This rapidly changing miscibility can explain the reverse trend between the 20 and 30 % C18:0 samples.

The comparison between 15 and 50 % RH reveals distinct differences. The 20/50/30 sample, which aged the least at 15 % RH, aged the most at 50 % RH. This increased ageing results mainly in the content of the lower phase. At high humidity, samples with a high OME content show the strongest ageing. The samples with a small OME content reveal with increasing C18:0 content the least ageing. This result can be explained by the increased polarity of samples with a high OME content. The higher the polarity, the greater the amount of water that can be dissolved in the fuel. The fact that the C18:0 content has a positive influence on ageing for the same OME content is attributable to the improved miscibility of the samples, which delays the formation of phase separation during ageing. When phase separation occurs, the different polarity of the fuel components changes the composition, which can then influence the ageing in a different way.

Compared to the C18:0 samples, the aged RME samples show a significantly more uniform ageing at 15 % RH. Samples 7/10/83 and 7/20/73, which fall within the poor miscibility range of the model, exhibit the greatest ageing. When the OME admixture is increased further to 30 %, miscibility is then improved. Sample 7/30/73, in comparison, shows the least ageing. It is interesting as regards RME ageing at 15 % RH that sample 50/30/20 exhibits no phase separation at a high RME content and, moreover, shows good ageing characteristics.

Fig. 14: Evaluation of ageing using the FTIR spectra, which are integrated according to equations 9 and 10 in the wave number range of the carbonyl band from 1580 to 1880 cm^{-1} and multiplied by the respective volume fraction of the phase.

Ageings at 50 % RH reveal, analogous to the C18:0 samples, a distinct difference. Sample 7/30/63 reveals, of all the 36 samples tested, the least ageing. Samples 7/10/83 and 7/20/73 exhibit at 50 % RH the most severe ageing. The trend derived from the

model that poorer miscibility leads to greater ageing is once more evident here. The improved miscibility at a higher RME content weakens the low oxidation stability of the unsaturated FAME molecules in combination with the OME content. Thus, sample 50/30/20 shows a comparable ageing as sample 30/30/40 despite the high RME content.

3.2.4 Dielectric relaxation spectroscopy

Another characterisation of ageing is offered by permittivity. The statements from the permittivity values differ from the FTIR results insofar as permittivity records the measured sample as a whole and, unlike FTIR, cannot distinguish between functional groups. Owing to the design of the ageing apparatus with a reflux condenser and the associated possible influx of water, permittivity values must be interpreted in terms of how great the proportion of water is in the result. Compared to the FTIR evaluations, the influence of water is stronger when it comes to permittivity. Water as a highly polar compound has a relative permittivity of $\varepsilon = 78$, which means that even small proportions of water produce a major change in the permittivity value. Analogous to the FTIR evaluation, ageing is calculated from the volume fractions (φ) of the phases and the permittivity values (ε_r') according to equations 11 and 12.

$$\text{Ageing index} = (\varepsilon_r'{}_{\text{ upper phase}} - \varepsilon_r'{}_{\text{ 0h}}) \cdot \varphi_{\text{ upper phase}} \qquad (11)$$

$$\text{Ageing index} = (\varepsilon_r'{}_{\text{ lower phase}} - \varepsilon_r'{}_{\text{ 0h}}) \cdot \varphi_{\text{ lower phase}} \qquad (12)$$

Fig. 15 depicts the ageing evaluations of the RME ageings for 15 and 50 % RH by means of permittivity. The contradictory results for sample 7/30/63 is revealed here at first glance. While sample 7/30/63 shows the least ageing in the FTIR evaluation, by far the highest ageing value can be found in terms of permittivity. The FTIR spectra of the sample show the large water or acid content to be in the OH band (>3100 cm^{-1}). The high water content of this sample makes it difficult to determine the degree of ageing by means of permittivity. This effect is enhanced by the fact that the changes in permittivity due to ageing are considerably lower for the samples with a higher polarity. For the other samples aged at 15 % RH it is evident that with a high OME content and an additional high RME content, the lower phase contributed almost entirely to ageing. Phase separation thus results in the concentration of the ageing products in the lower phase. Sample 50/30/20 shows the least ageing in the evaluation with the permittivity.

At the same time, this sample exhibits no phase separation and is likewise promising when evaluating ageing with FTIR.
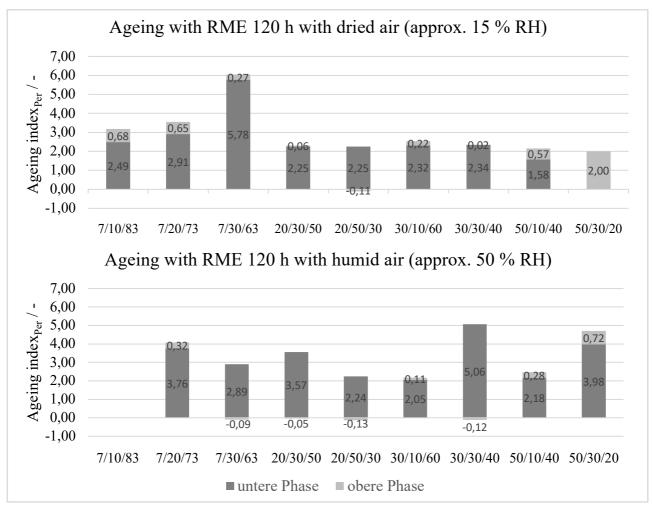

Fig. 15: Evaluation of ageing according to equations 11 and 12 using permittivity and volume fraction.

When the RME samples are aged at 50 % RH, the concentration of the ageing products increases in the lower phase, which is proven by the negative permittivity difference in the majority of the upper phases. This means that during ageing, polar products (RME, C18:0, OME and polar ageing products) diffuse from the upper to the lower phase. This effect cannot be observed from the evaluations with the FTIR measurement technique, which proves that when analysing ageing products, several study methods must be used for a complete evaluation of the fuel ageings. A uniform trend, as it occurs in the other evaluations, cannot be observed here.

A characterisation of ageing in the C18:0 samples is possible for the upper phases only. Since only the sum of the upper and lower phase can yield reliable results for evaluating ageing, permittivity cannot be evaluated for the C18:0 samples. The reason for the non-evaluable permittivity measurements of the C18:0 samples is the relaxation that occurs

in the aged lower phases with C18:0 (Fig. 16). The relaxation, which usually lies outside the measuring range of the sensor, migrates into the measuring range between 5 and 100 kHz for reasons that have not yet been clarified. This is why it is not possible to evaluate permittivity at 1 MHz or at other frequencies.
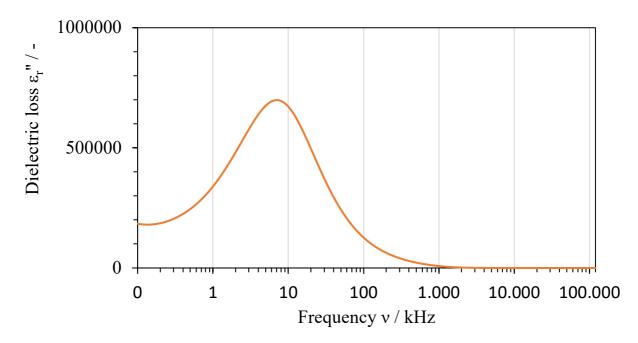

Fig. 16: Dielectric losses of the C18:0 7/10/83 sample aged at 50 % RH for 120 h. The relaxation results in non-evaluable permittivity values of the lower phases of the C18:0 samples.

The relaxation characterises the dielectric losses that occur when the molecules' orientation can no longer follow the applied alternating field. These losses cause a shift in the resonant frequency of the sensor, whereby no permittivity can be output at 1 MHz (Fig. 17).

The results of the evaluation on ageing at different humidities reveal that the greater polarity of the regenerative fuel blends exacerbates the issue of storage conditions when compared to fossil fuels. Likewise, the greater differences in polarity and the resulting limited miscibility of HVO and OME, for example, can also lead to new influences on ageing. Depending on how sharply polarity is increased through oxidation, water concentration can vary greatly. For these reasons, studies into the cross influences of the blend components on ageing and the increased influx of water should be an integral part of any further research.
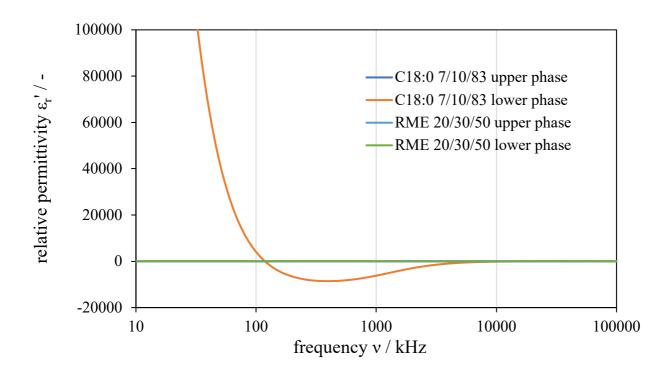
Fig. 17: Non-evaluable relative permittivity of the aged C18:0 samples (50 % RH) when compared to the evaluable samples of the aged RME samples. The negative range is a result of the sensor's resonance shift caused by the relaxation.

4   Summary

Blending different regenerative fuels presents a challenge when it comes to large differences in polarity. A well-known example is the desegregation of hydrated vegetable oil (HVO) and polyoxymethylene dimethyl ether (OME). At this point, one promising idea is to use ternary blends that add rapeseed oil methyl ester (RME) as a solubiliser. In the project "Biodiesel as an integral component of pioneering diesel fuels", this aspect is studied in two project parts.

The first part of the project studied the miscibility of OME, HVO and RME blends or OME, HVO and C18:0 blends with the help of experimental tests and numerical calculations. Comparing these measurements reveals the difference between RME and C18:0 (stearic acid methyl ester). The calculations were made based on Hansen's theory, which states that fuels only stay blended when the properties of the blended fuels do not different significantly from one another. The results of the Hansen's calculations reveal that, depending on the polarity of the ternary blends, miscibility can be positively influenced by RME. Depending on the proportion of the nonpolar

component, HVO, the admixture of RME must be adapted accordingly in order to achieve optimum miscibility. While segregation can be observed at low temperatures for low RME admixtures of less than 10 % and a high HVO content, blends of equal proportions of RME, OME and HVO obtain stable blends across the entire temperature range. This means that RME provides a positive influence on blend stability of the ternary blends for non-aged blends of OME, HVO and RME.

In the second part of the project, ageing tests were conducted with selected fuel blends on an apparatus developed in Coburg. The apparatus permits the controlled ageing of fuels at defined temperatures, durations, oxygen mixing and influx of moisture. In the context of ageing, 9 different blends, 2 air dehumidification grades as well as RME and C18:0 samples were tested, so that a total of 36 different ageings with an ageing period of 120 h are examined. The results reveal that the miscibility of the fuel blends must be reassessed due to the oxidation during ageing. Thus, apart from one exception, phase separations occur in all aged samples at 110 °C and at an ageing period of 120 h. If the unaged fuel mixture has a sufficiently high polarity, as is the case in the sample with 50 % RME, 30 % OME and 20 % HVO, then no phase separation could be observed. This applies to the case that the influx of water into the fuel is kept low during ageing.

Due to the new ageing apparatus, a system has been created that can introduce a considerable amount of water into the aged samples. In order to study the influence of water on ageing, each sample was subjected to a further ageing in which the air was pre-dried. The higher water content in the samples leads to a significant influx of water over the ageing period when the polarity is high (for samples with 30% OME admixture). The degree of ageing, derived from the carbonyl oscillation in the infrared spectrum, was influenced only slightly. All samples exhibited a concentration of the ageing products in the lower phase, whereas the upper phase differed only slightly from the unaged samples in the IR spectrum and in permittivity. This small difference can be explained by two processes. The polar, unaged OME proportion concentrates in the lower phase during a phase separation, thus decreasing the polarity of the upper phase. Oxidation products with only a low polarity partially pass into the upper phase, which again increases their polarity. Under humid conditions, therefore, water is concentrated in the lower phase during ageing.

Using C18:0 did not result in any significant change in the test results. Miscibility was verified with both solubilisers, and the ageing behaviour also revealed no fundamental improvement or deterioration of the results in the described measurement setup. In some tests, however, crystallisation was detected in the samples containing C18:0. This
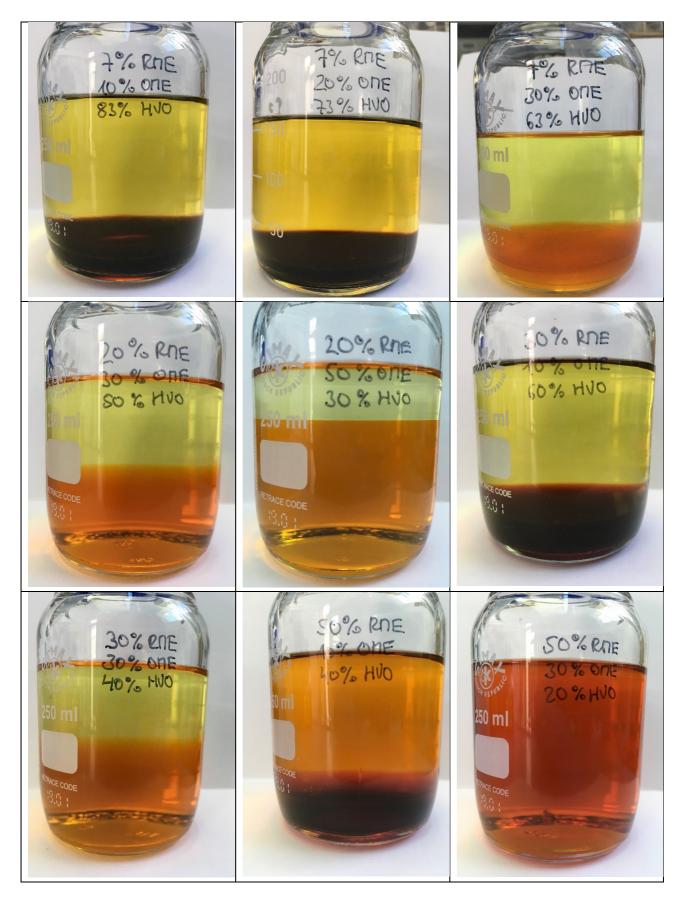
crystallisation during ageing corresponds to the known poorer cold properties of C18:0 when compared to RME.

To sum up, it can be said that increased admixtures of RME have a positive influence on the segregation stability of unaged OME, HVO and RME samples. No phase separations could be detected in the unaged condition for mixtures of at least 7 %. For very aged samples, the admixture of RME can only prevent segregation when at least 50 % RME is present in the mixture.
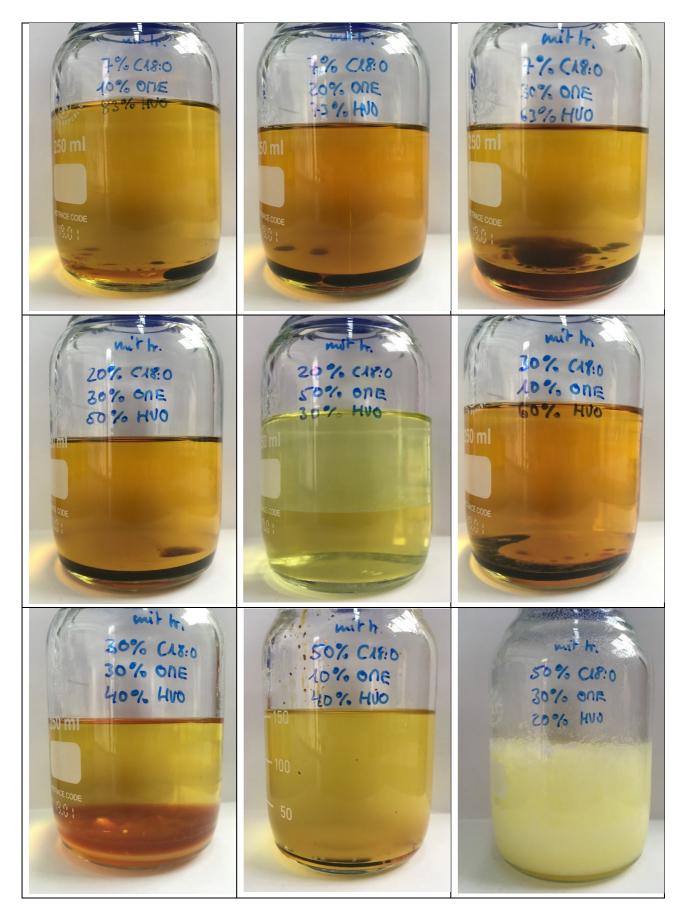
Initial positive results for the deployment of RME as a solubiliser in fuels with widely varying polarities have been recorded by the studies conducted here. However, several questions still need to be resolved for any real deployment of such ternary blends in vehicles. This includes, among other things, the exact ageing process, but also material compatibilities with fuel-carrying components.

5   Annex

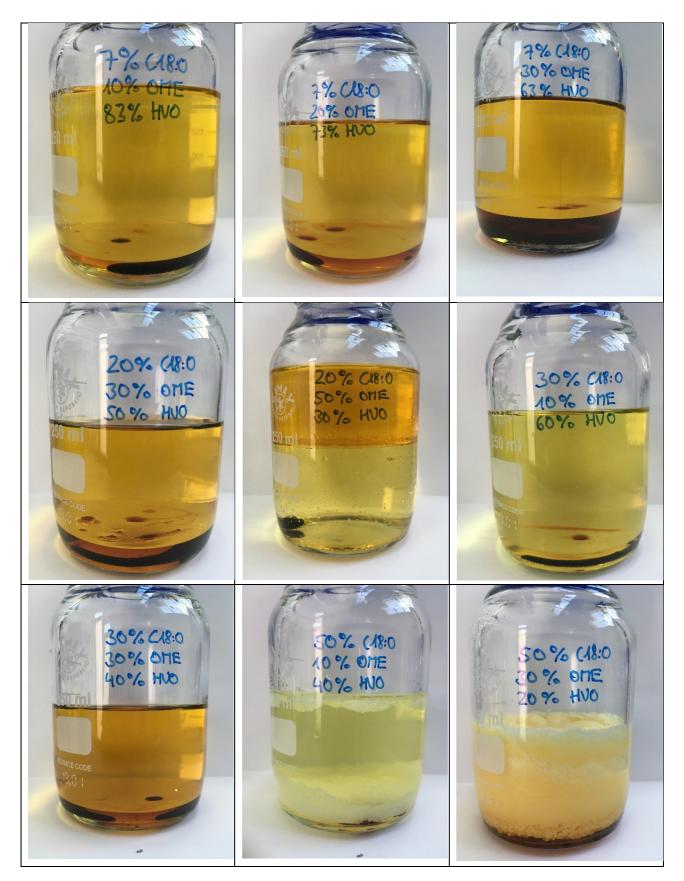RME: Ageing 120 h at 15 % relative humidity

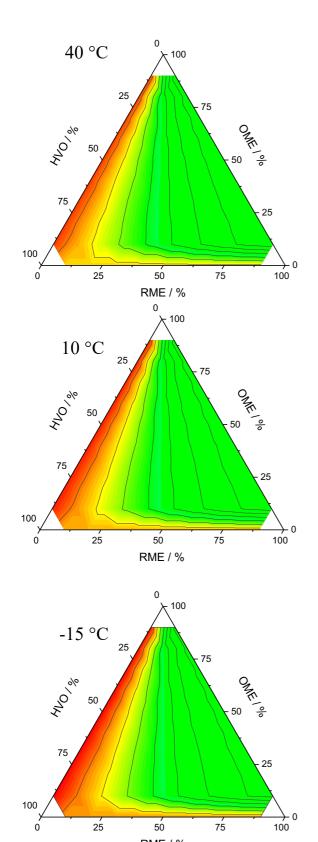C18:0 ageing 120 h at 15 % relative humidity

RME ageing 120 h at 50 % relative humidity
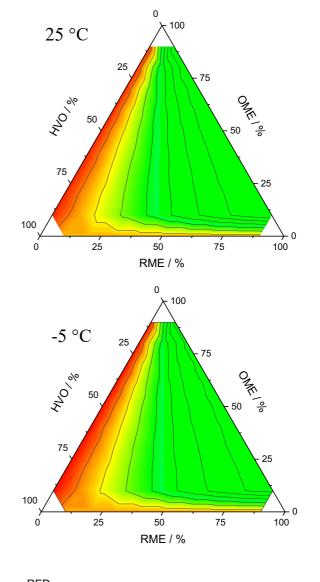
C18:0 ageing 120 h at 50 % relative humidity

Miscibility model: Relative energy distance (RED) for blends of RME, OME and HVO at 40 °C to -15 °C.
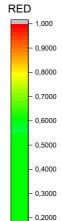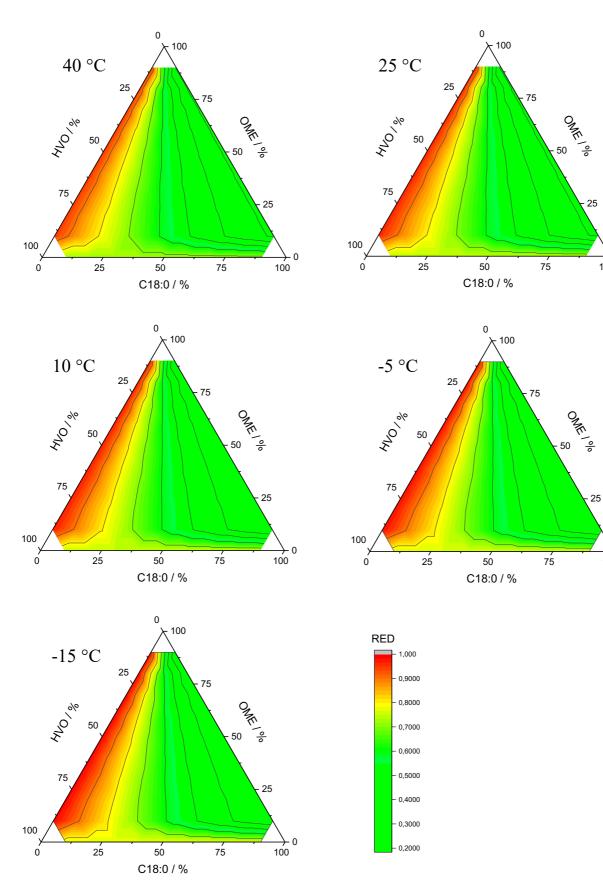
Miscibility model: Relative energy distance (RED) for blends of C18:0, OME and HVO at 40 °C to -15 °C.

6 Literary references

[1] O.P. Bhardwaj, A. F. Kolbeck, T. Kkoerfer, M. Honkanen; Potential of Hydrogenated Vegetable Oil (HVO) in Future High Efficiency Combustion System SAE International Journal of Fuels and Lubricants, Vol. 6, No. 1 (April 2013), pp. 157-169.

[2] H. Pflaum, P. Hofmann, B. Geringer, W. Weissel, "Potential of Hydrogenated Vegetable Oil (HVO) in a Modern Diesel Engine," SAE Technical Paper 2010-32-0081, 2010.

[3] M. Härtl, K. Gaukel, D. Pélerin, G. Wachtmeister, Oxymethylenether als potenziell CO2-neutraler Kraftstoff für saubere Dieselmotoren; MTZ 78,2017, 2, 52–58.

[4] B. Lumpp, D. Rothe, C. Pastötter, R. Lämmermann, E. Jacob; Oxymethylenether als Dieselkraftstoffzusätze der Zukunft; MTZ 72, 2011, 198–202.

[5] T. Garbe, M. Hönig, W. Kaszas, J. Klose, H. Bröker, E. Pott, Influence of Power to Liquid Fuels on the Emissionsof modern Passenger Cars. 10th Int. AVL Exhaust Gas and Particulate Emissions Forum.

[6] A. Datta, B. K. Mandal; A comprehensive review of biodiesel as an alternative fuel for compression ignition engine; Renew Sust Energy Rev. 2016, 57, 799–821.

[7] G. Dwivedi, S. Jain, M.P. Sharma; Impact analysis of biodiesel on engine performance–A review; Renew Sust Energy Rev. 2011, 15, 4633–4641.

[8] J. E, M. Pham, D. Zhao, Y. Deng, D. Le, W. Zuo, H. Zhu, T. Liu, Q. Peng, Z. Zhang; Effect of different technologies on combustion and emissions of the diesel engine fuelled with biodiesel: A review; Renew Sust Energy Rev. 2017, 620–647.

[9] M. F. Othman, A. Adam, G. Najafi, R. Mamat; Green fuel as alternative fuel for diesel engine: A review; Renew Sust Energy Rev. 2017, 694–709.

[10] C. M. Hansen, Theuniversality of the solubility parameter; Ind. Eng. Chem. Prod. Res. Dev. 1969, 8, 1, 2-11.

[11] T. B. Nielsen, C. M. Hansen; Elastomer swelling and Hansen solubility parameters; Polymer Testing, 2005, 24, 1054–1061.

[12] A. Beerbower, P.L. Wu, A. Martin; Expanded solubility parameter approach. I: Naphthalene and benzoic acid in individual solvents. J. Paint Technol. 1884, 43, 35–42.

[13]   C. M. Hansen; "Solubility Parameters," in *Paint and Coating Testing Manual: 15th. Edition of the Gardner-Sward Handbook*, ed. J. Koleske (West Conshohocken, PA: ASTM International, 2012), 470-494.

[14] J.Ernst, W.S. Sheldrick, J.H. Fuhrhop; Die Strukturen der essentiellen ungesättigten Fettsäuren, Kristallstruktur der Linolsäure sowie Hinweise auf die Kristallstrukturen der α-Linolensäure und der Arachidonsäure; Z. Naturforsch. 1979, 34b, 706-711.

ufop